Weak-triplet, color-octet scalars, and the CDF dijet excess

Bogdan A. Dobrescu and Gordan Z. Krnjaic

Phys. Rev. D **85**, 075020 — Published 24 April 2012

DOI: 10.1103/PhysRevD.85.075020

FERMILAB-PUB-11-141-T

Weak-triplet, color-octet scalars and the CDF dijet excess

Bogdan A. Dobrescu[1] and Gordan Z. Krnjaic[1,2]

1) *Theoretical Physics Department, Fermilab, Batavia, IL 60510, USA*

2) *Department of Physics and Astronomy, Johns Hopkins University, Baltimore, MD 21218, USA*

April 14, 2011; revised June 24, 2011

We extend the standard model to include a weak-triplet and color-octet scalar. This 'octo-triplet' field consists of three particles, two charged and one neutral, whose masses and renormalizable interactions depend only on two new parameters. The charged octo-triplet decay into a W boson and a gluon is suppressed by a loop factor and an accidental cancellation. Thus, the main decays of the charged octo-triplet may occur through higher-dimensional operators, mediated by a heavy vectorlike fermion, into quark pairs. For an octo-triplet mass below the $t\bar{b}$ threshold, the decay into $Wb\bar{b}$ or $Wb\bar{s}$ through an off-shell top quark has a width comparable to that into $c\bar{s}$ or $c\bar{b}$. Pair production with one octo-triplet decaying into two jets and the other decaying into a W and two soft b jets may explain the dijet-plus-W excess reported by the CDF Collaboration. Using a few kinematic distributions, we compare two mechanisms of octo-triplet pair production: through an s-channel coloron and through the coupling to gluons. The higher-dimensional operators that allow dijet decays also lead to CP violation in $B_s - \overline{B}_s$ mixing.

1 Introduction

Scalar fields transforming as octets under $SU(3)_c$, the color group of the strong interactions, have been studied in various contexts. The simplest type of color-octet scalar is a singlet under the $SU(2)_W$ group of the weak interactions, and may be referred to as an 'octo-singlet'. These lead to pairs of dijet resonances at hadron colliders [1, 2], and may explain [3] some deviations from the standard model predictions in the $3b$ search performed by the CDF collaboration [4]. They also enhance the standard model Higgs boson production through gluon fusion [5]. Octo-singlets appear as composite particles due to technicolor [6] and other strong-coupling dynamics [7, 8], or as elementary particles in 6-dimensional extensions of the standard model [9] and in theories with an extended color group [3, 10].

Weak-doublet color-octet scalars (*i.e.*, 'octo-doublets') differ dramatically from octo-singlets because the standard model gauge symmetry allows renormalizable couplings of octo-doublets to the standard quarks [11]. Only if these couplings are highly suppressed or aligned with the standard model Yukawa couplings can the octo-doublets be light enough to be produced at the LHC [12]. An octo-doublet field includes four color-octet states: a charged particle, a neutral one and their antiparticles. The hadron collider signatures of octo-doublets have been explored in [13, 14].

In this paper we study 'octo-triplets': real scalar fields that transform in the adjoint representation, $(8, 3, 0)$, of $SU(3)_c \times SU(2)_W \times U(1)_Y$. An octo-triplet field includes three color-octet states: a particle of charge $+1$, its antiparticle, and a neutral real particle. Akin to octo-singlets, octo-triplets are pair produced at hadron colliders through their couplings to gluons, and cannot decay into standard model fermions at renormalizable level because the Yukawa couplings are not $SU(2)_W \times U(1)_Y$ invariant. Unlike octo-singlets, octo-triplets cannot decay into gluons unless there are additional fields that generate certain dimension-7 operators.

One-loop decays of octo-triplets into a gluon and an electroweak boson are allowed, leading to interesting collider signatures involving two gluons and two electroweak bosons. We will show, however,

that the rate of these decays is accidentally suppressed by two orders of magnitude compared to usual 1-loop estimates. Thus, new heavy particles could induce the dominant octo-triplet decay modes.

In the presence of some vectorlike quark of mass in the TeV range, the charged octo-triplet may decay into a pair of standard model quarks, or into a W boson and a pair of quarks if it is lighter than the top quark. This leads to a variety of collider signatures, including a dijet resonance, a W boson and two softer jets. If the octo-triplet mass is in the 150 – 170 GeV range, this signature may explain the 4.1σ excess observed by the CDF Collaboration in the dijet resonance plus W final state [15, 16][1]. Some alternative explanations can be found in [3],[18]-[20]. At the LHC, octo-triplets with much larger masses ($\sim$1 TeV) may be probed in several final states.

Octo-triplets may be elementary particles (*e.g.*, part of the 75 representation of $SU(5)$ grand unification), or may arise as composite ones, for example as fermion-antifermion bound states [8]. We treat the octo-triplets as point-like particles, which is a good approximation only when the compositeness scale is substantially higher than the octo-triplet mass.

In Section 2 we analyze the extension of the standard model by one real octo-triplet field. Section 3.1 introduces a heavy vectorlike quark which mediates octo-triplet decays into standard model quarks. Section 3.2 discusses flavor-changing processes. The Tevatron phenomenology of charged octo-triplets is explored in sections 3.3 (QCD pair production) and 3.4 (resonant pair production). The predictions for LHC are discussed in section 3.5. Our conclusions are summarized in Section 4. In the appendices we present the Feynman rules for octo-triplets, and then we compute the rates for the 3-body weak decay of the charged octo-triplet and for the 2-body 1-loop decays of color-octet scalars.

2 Octo-triplet scalar

We consider the standard model plus an octo-triplet, $\Theta^{a\alpha}$, which is a real field of spin 0 transforming as $(8,3,0)$ under the standard $SU(3)_c \times SU(2)_W \times U(1)_Y$ gauge group. We use indices from the beginning of the Roman and Greek alphabets to label the $SU(3)_c$ and $SU(2)_W$ generators, respectively: $a,b,c = 1,\ldots,8$ and $\alpha,\beta,\gamma = 0,1,2$.

[1]The D0 search in the same channel [17] has a larger background and less data, so that it might not be sensitive enough to the signature proposed here.

2.1 Interactions and masses

All interactions of the octo-triplet with standard model gauge bosons are contained in the kinetic term

$$\frac{1}{2}\left(D_\mu \Theta^{a\alpha}\right)\left(D^\mu\,\Theta^{a\alpha}\right) \quad , \tag{2.1}$$

where μ is a Lorentz index and the covariant derivative is given by

$$D_\mu \Theta^{a\alpha} = \partial_\mu \Theta^{a\alpha} + g_s f^{abc} G^b_\mu \Theta^{c\alpha} + g\epsilon^{\alpha\beta\gamma} W^\beta_\mu \Theta^{a\gamma}. \tag{2.2}$$

Here f^{abc} and $\epsilon^{\alpha\beta\gamma}$ are the totally antisymmetric tensors of the $SU(3)_c$ and $SU(2)_W$ groups, respectively, g_s and g are the $SU(3)_c \times SU(2)_W$ gauge couplings, G^a_μ is the gluon field, and W^α_μ is the weak gauge field. The octo-triplet field includes three particles: an electrically-neutral color-octet real scalar Θ^{a0}, a color-octet scalar of electric charge $+1$, Θ^{a+}, and its antiparticle Θ^{a-}:

$$\Theta^{a\pm} = \frac{1}{\sqrt{2}}\left(\Theta^{a1} \mp i\Theta^{a2}\right) \quad . \tag{2.3}$$

When referring informally to the octo-triplet particles we use the $\Theta^\pm$ and Θ^0 symbols without displaying the color index a.

The kinetic term (2.1) includes interactions of the W boson with two octotriplet particles,

$$-igW^-_\mu\left[(\partial_\mu\Theta^{a+})\Theta^{a0} - \Theta^{a+}\partial_\mu\Theta^{a0}\right] + \text{H.c.} \quad , \tag{2.4}$$

and also with an additional gluon:

$$2igg_s f^{abc}\, G^{\mu a}\left(W^+_\mu\Theta^{b-} - W^-_\mu\Theta^{b+}\right)\Theta^{c0} \quad . \tag{2.5}$$

Similar interactions involve a Z boson and two octotriplet particles of the same charge, with or without an additional gluon. The interactions of like-sign octo-triplets with one or two gluons (photons) are completely specified by QCD (QED) gauge invariance. The Feynman rules for octo-triplets are given in Appendix A.

The mass of the octo-triplet arises from two terms in the Lagrangian:

$$-\frac{1}{2}\left(M_0^2 - \lambda_H H^\dagger H\right)\Theta^{a\alpha}\Theta^{a\alpha} \quad , \tag{2.6}$$

where λ_H is a real dimensionless parameter. The VEV of the standard model Higgs doublet H has a value $v_H \simeq 174$ GeV, so that the mass of the octo-triplet field is

$$M_\Theta = \sqrt{M_0^2 - \lambda_H v_H^2} \quad . \tag{2.7}$$

We require $M_\Theta > 0$ (*i.e.,* $\Theta^{a\alpha}$ does not acquire a VEV) in order to preserve $SU(3)_c$ gauge invariance. Note that Higgs searches based on gluon fusion place a limit on λ_H as a function of M_Θ [5].

The commutation relations of the Pauli matrices σ^α imply that other operators contributing to the octo-triplet mass, such as $(H^\dagger\sigma^\alpha\sigma^\beta H)\Theta^{a\alpha}\Theta^{a\beta}$, are either identical to the last one in Eq. (2.6) or vanish. Thus, at tree level $\Theta^\pm$ and Θ^0 are degenerate states, having masses equal to M_Θ. At one loop, the electroweak interactions break this degeneracy. The mass splitting between the charged and neutral octo-triplets is [21]

$$\delta M \equiv M_{\Theta^+} - M_{\Theta^0} \simeq \frac{1-\cos\theta_W}{2\sin^2\theta_W}\alpha M_W \tag{2.8}$$

up to corrections of order $(M_W/M_\Theta)^2$. We will see shortly that the octo-triplets have lifetimes much longer than the QCD scale, so that they hadronize. The lightest physical states are "octo-hadrons" given by a Θ^0 or $\Theta^\pm$ bound to gluons or quark-antiquark pairs. The mass difference δM between the lightest charged and neutral octo-hadrons is of the same sign and order of magnitude as $M_{\Theta^+} - M_{\Theta^0}$, so that $\delta M \sim 0.2$ GeV.

$SU(2)_W \times U(1)_Y$ gauge-invariance forbids any renormalizable interaction of the octo-triplet with standard model fermions. The most general renormalizable Lagrangian ($\mathcal{L}_\Theta$) for the octo-triplet scalars is given by the kinetic term (2.1), the potential terms quadratic in Θ given in Eq. (2.6), as well as a cubic term and quartic terms:

$$\mu_\Theta f^{abc}\epsilon^{\alpha\beta\gamma}\Theta^{a\alpha}\Theta^{b\beta}\Theta^{c\gamma} - \lambda_\Theta\left(\Theta^{a\alpha}\Theta^{a\alpha}\right)^2 \quad , \tag{2.9}$$

where $\lambda_\Theta > 0$ is a dimensionless parameter, and for simplicity we display only one quartic term. The mass parameter μ_Θ may be positive or negative, but its size should not be larger than $O(M_\Theta\lambda_\Theta^{-1/2})$ in order to prevent a Θ VEV. The above cubic term gives the following interaction among the charged and neutral octo-triplet particles:

$$2i\mu_\Theta f^{abc}\Theta^{a+}\Theta^{b-}\Theta^{c0} \quad . \tag{2.10}$$

2.2 Collider signals of octo-triplets

In the $\mu_\Theta \to 0$ limit, the Lagrangian $\mathcal{L}_\Theta$ has an accidental $\mathcal{Z}_2$ symmetry that makes the lightest octo-triplet (*i.e.,* Θ^0) stable. The charged octo-triplet decays at tree level into Θ^0 and an off-shell W boson. Computing the 3-body width to leading order in δM (Appendix B) we find

$$\Gamma\left(\Theta^\pm \to \Theta^0 e^\pm \nu\right) \simeq \frac{\alpha^2}{15\pi\sin^4\theta_W}\frac{(\delta M)^5}{M_W^4} \, . \tag{2.11}$$

Given the small mass splitting $\delta M \sim 0.2$ GeV [see the comment after Eq. (2.8)], the only other relevant decay mode is $\Theta^\pm \to \Theta^0\mu^\pm\nu$ with a decay width further phase-space suppressed compared to Eq. (2.11). Hence, the total tree-level width of $\Theta^\pm$ is $\Gamma_{\rm tree}(\Theta^\pm) \simeq 1.8\times10^{-16}$ GeV. This 3-body decay width corresponds to a decay length of 1.1 cm.

For $\mu_\Theta \neq 0$, the charged octo-triplet decays into gauge bosons at one loop, with Wg being the only 2-body final state allowed by charge conservation. The diagrams responsible for this decay are shown in Figure 1. The computation of the decay width described in Appendix C gives

$$\Gamma\left(\Theta^\pm \to W^\pm g\right) \simeq \frac{\alpha\alpha_s\mu_\Theta^2}{\pi^3\sin^2\theta_W M_\Theta} f(M_W/M_\Theta) \, , \tag{2.12}$$

where the function $f(R)$ is defined in Eq. (C.8). For M_Θ varying between 150 GeV and 1 TeV, $f(R)$ grows from $(4.0 - 10.3)\times10^{-3}$, corresponding to $\Gamma(\Theta^\pm \to W^\pm g)$ in the $(4.3{-}11.2)\times10^{-7}\mu_\Theta^2/M_\Theta$ range. While one might naively expect $f(R)$ to be of order one, this function is accidentally suppressed: $f(0) \propto \left(\pi^2/9 - 1\right)^2$ as shown in Eq. (C.10), while for larger values of R, the function decreases further due to phase space suppression.

The neutral octo-triplet also decays at one loop, into a gluon and Z boson or photon, with partial widths

$$\Gamma\left(\Theta^0 \to Zg\right) \simeq \frac{\alpha\alpha_s\mu_\Theta^2}{\pi^3\tan^2\theta_W M_\Theta} f(M_Z/M_\Theta) \quad ,$$
$$\Gamma\left(\Theta^0 \to \gamma g\right) \simeq \frac{\alpha\alpha_s\mu_\Theta^2}{\pi^3 M_\Theta} f(0) \, . \tag{2.13}$$

When M_Θ varies between 150 GeV and 1 TeV, the branching fraction for $\Theta^0 \to \gamma g$ decreases from 53% to 24%. The decay $\Theta^0 \to gg$ does not occur at one loop due to $SU(2)_W$ invariance (this decay requires

a dimension-7 operator involving two Higgs fields; furthermore the $(H^\dagger H)\Theta^{a\alpha}\Theta^{a\alpha}$ interaction does not change the $SU(2)_W$ indices, so that Higgs Yukawa couplings must be inserted, which is possible only at three loops).

At hadron colliders, octo-triplets are copiously pair produced due to their QCD couplings to gluons. The rate for $\Theta^0\Theta^0$ production is the same as for an octo-singlet of same mass [2, 3], while $\Theta^+\Theta^-$ production is twice as large (additional contributions due to photon and Z exchange are negligible). In Figure 2 we show the leading order $\Theta^+\Theta^-$ production cross section at the Tevatron and LHC, computed with MadGraph 5 [22] (with model files generated by FeynRules [23]) using the CTEQ 6 parton distribution functions [24]. The QCD corrections are not included in this plot; we expect their inclusion to shift these curves upwards by $O(50\%)$.

Note that single octo-triplet production (through diagrams similar to those in Figure 1) is negligible because it is suppressed by a loop factor, the weak coupling constant, and $(\mu_\Theta/M_\Theta)^2$.

The $\Theta^0\Theta^0$ pair leads to $(Zj)(Zj)$, $(\gamma j)(Zj)$ and $(\gamma j)(\gamma j)$ final states, where j is a gluonic jet and the parantheses indicate that the two objects form a resonance of mass M_Θ. The $\Theta^+\Theta^-$ pair leads to $(W^+j)(W^-j)$ final states, unless $\mu_\Theta^2/M_\Theta \lesssim O(10^{-9})$ GeV which leads to a large branching fraction for the $\Theta^\pm \to \Theta^0 e^\pm \nu$ decay. This latter case gives the same final state as in $\Theta^0\Theta^0$ production because the electron and neutrino are very soft and most likely do not pass the cuts (even when $\Theta^\pm$ is boosted the electron is not isolated). If $\mu_\Theta^2/M_\Theta \simeq 4\times10^{-10}$ GeV, then the 2- and 3-body decays of $\Theta^\pm$ have comparable widths, so that the $\Theta^+\Theta^-$ pair leads to

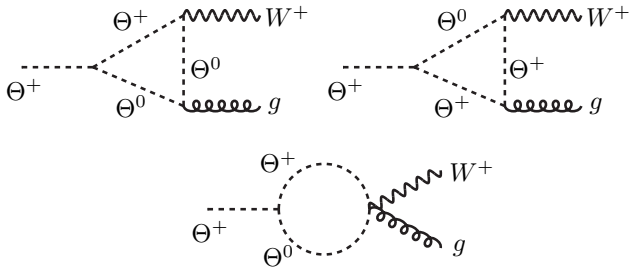

Figure 1: Charged octo-triplet decay to a W boson and a gluon.

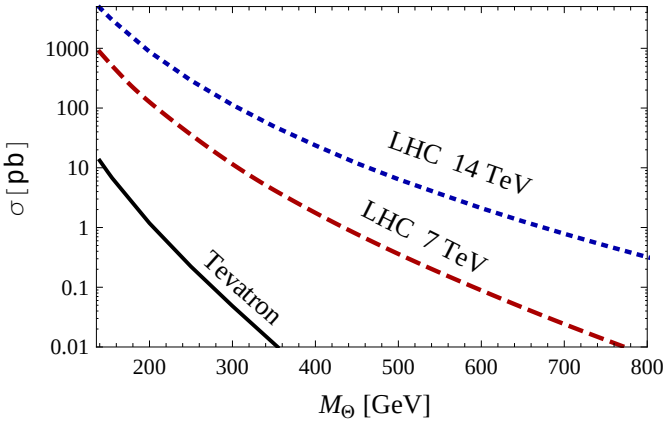

Figure 2: Leading order cross section for charged octo-triplet pair production at the Tevatron (black solid line) and LHC at $\sqrt{s} = 7\,\text{TeV}$ (red dashed line) and at $\sqrt{s} = 14\,\text{TeV}$ (blue dotted line).

$(Wj)(Zj)$ and $(Wj)(\gamma j)$ final states, with the (Zj) and (γj) vertices originating from displaced vertices.

Let us briefly discuss the $(W^+j)(W^-j)$ signal at the LHC, where the production cross section, Figure 2, can be very large. This final state is most easily identified when one W decays leptonically while the other decays hadronically with an overall $W+4j$ signature. The W decay products reconstruct W resonances and can thereby be isolated from the other jets in the event. These remaining jets can then be grouped alongside the known W decay products and used to reconstruct pairs of octo-triplet resonances. Backgrounds to this signature include $W+$ jets production and $t\bar{t}$ pair-production, the latter of which can be substantially reduced by anti-b tagging.

Besides nonresonant pair production, octo-triplet scalars may induce resonant signatures at hadron colliders because, like other long-lived colored particles [25, 26], they form bound states. If the octo-triplet width is much less than the binding energy $E_\mathcal{B}$ due to gluon exchange, then bound states form before either particle decays. This is the case for all values of M_Θ and μ_Θ, as the dominant 2-body octo-triplet width given in Eq. (2.12) easily satisfies

$$\Gamma(\Theta^\pm \to W^\pm g) \ll E_\mathcal{B} = \frac{9}{4}\alpha_s^2\, M_\Theta\ , \qquad (2.14)$$

For simplicity, we consider only the formation of color-singlet bound states $\mathcal{B}$; this is the dominant

channel and our qualitative conclusions apply to different color-representations of bound states.

The bound states annihilate into gauge-boson pairs before either constituent decays. Bound states of neutral octo-triplets can only annihilate through the processes $\Theta^0\Theta^0 \to \mathcal{B} \to gg, W^+W^-$, while the annihilation of bound states of charged octo-triplets yields a rich variety of vector boson pairs: $\Theta^+\Theta^- \to \mathcal{B} \to gg, W^+W^-, ZZ, \gamma\gamma, \gamma Z$.

Given that the bound-state effects are mainly due to gluon exchange, the production of the $\Theta^+\Theta^-$ bound state is approximately equal to that of octo-singlets computed in [8]: for $M_\Theta \approx 150\,\text{GeV}$ the Tevatron cross section is $\sigma(p\bar{p} \to \mathcal{B}) \simeq O(100)\,\text{fb}$. Since the width $\Gamma(\Theta^\pm \to W^\pm g)$ is orders of magnitude smaller than the main channel for bound states $\Gamma(\mathcal{B} \to gg) \simeq 0.04\,\text{GeV}$ [8], the annihilation dominates and yields dijet resonances with invariant mass $M_\mathcal{B} = 2M_\Theta - E_\mathcal{B}$. This cross section is too small to be observed at the Tevatron.

At the LHC, the bound state production cross-section can be considerably larger. For $M_\mathcal{B} \sim 1\,\text{TeV}$, the cross section is $\sigma(pp \to \mathcal{B}) \sim O(1\,\text{pb})$ [26] at $\sqrt{s} = 14\,\text{TeV}$, which might allow the annihilation signal to compete with the QCD background and give an observable resonance. The electroweak diboson channels are suppressed relative to gg, but give cleaner signals, which contribute to standard Higgs searches.

While the above discussion has been limited to the dominant color-singlet bound state, octo-triplets can also form bound states in higher color representations with exotic annihilation signatures. For instance, color-octet bound states annihilate into either γg or Zg regardless of whether the bound state comprises charged or neutral scalars.

3 Octo-triplet decays via higher-dimensional operators

Since the octo-triplet widths in Eqs. (2.11)-(2.12) are tiny, higher-dimensional operators induced at the TeV scale could lead to other decays with substantial branching fractions.

Dimension-5 operators allow the coupling of an octo-triplet to a pair of standard model quarks involving a derivative,

$$\frac{c_{ij}}{m_\psi}\,\Theta^{a\alpha}\,\overline{Q}_L^{\,i}\,T^a\,\frac{\sigma^\alpha}{2}\gamma^\mu D_\mu Q_L^{\,j} + \text{H.c.}\quad , \tag{3.1}$$

or in the presence of the Higgs doublet,

$$\Theta^{a\alpha}\,\overline{Q}_L^{\,i} T^a \frac{\sigma^\alpha}{2}\left(\frac{c'_{ij}}{m_\psi}\widetilde{H}u_R^j + \frac{c''_{ij}}{m_\psi}Hd_R^j\right)\quad . \tag{3.2}$$

Q_L^i, u_R^j and d_R^j are the quark fields in the gauge eigenstate basis; $i,j = 1,2,3$ label the fermion generation; σ^α is a Pauli matrix; m_ψ is the mass of some heavy field that has been integrated out; and c_{ij}, c'_{ij} and c''_{ij} are dimensionless coefficients. Using the field equations, one can replace the last operator, with coefficient c''_{ij}, by a linear transformation (involving the standard model Yukawa couplings) of the c_{ij} and c'_{ij} coefficients.

3.1 Octo-triplet plus a vectorlike quark

The dimension-5 operators (3.1) and (3.2) can be induced, for example, by a heavy vectorlike quark Ψ that transforms as $(3,2,1/6)$ under $SU(3)_c \times SU(2)_W \times U(1)_Y$, *i.e.* the same way as SM quark doublets Q_L^i. Renormalizable interactions of Ψ with the octo-triplet,

$$\mathcal{L}_{\Theta\Psi} = \Theta^{a\alpha}\,\overline{\Psi}_R\,T^a\frac{\sigma^\alpha}{2}\left(\eta_i Q_L^i + \eta_\psi \Psi_L\right) + \text{H.c.}\ , \tag{3.3}$$

and with the Higgs doublet,

$$\mathcal{L}_{H\Psi} = \overline{\Psi}_L\left(\lambda_i^u\,H u_R^i + \lambda_i^d\,\widetilde{H}d_R^i\right)\quad , \tag{3.4}$$

are allowed. Here η_i, η_ψ, λ_i^u and λ_i^d are dimensionless couplings and $\widetilde{H} = i\sigma^2 H^\dagger$. Gauge-invariant fermion mass terms are also allowed:

$$-\,m_\psi\overline{\Psi}_L\Psi_R - \mu_i\overline{Q}_L^{\,i}\Psi_R + \text{H.c.} \tag{3.5}$$

For $m_\psi \gg M_\Theta$, the Ψ fermion can be integrated out, giving rise to the operators (3.1) through the $\mathcal{L}_{\Theta\Psi}$ interactions, and to the operators (3.2) through a combination of $\mathcal{L}_{\Theta\Psi}$ and $\mathcal{L}_{H\Psi}$ interactions.

Let us assume for simplicity that λ_i^u and λ_i^d are negligible, and that the mass mixing parameters satisfy $\mu_i \ll m_\psi$. In this case the coefficients c_{ij} can be computed in the mass insertion approximation:

$$c_{\,ij} = -\frac{i\,\eta_i^*\mu_j}{m_\psi}\quad . \tag{3.6}$$

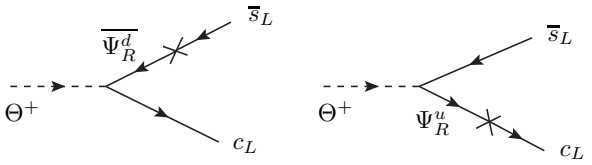

Figure 3: Charged octo-triplet decay to quarks in the presence of a vectorlike quark doublet $\Psi = (\Psi^u, \Psi^d)$. The mass mixing of Ψ with the standard model quarks is depicted by $\times$. Similar diagrams lead to the decay of the neutral Θ^0 scalar into quark pairs.

These are the coefficients at the scale m_ψ; running down from m_ψ to M_Θ may change c_{ij} at M_Θ by an $O(1)$ factor, which we can absorb into the definition of η_i.

Using the quark field equations, we find that Eq. (3.1) contains the following interactions between Θ^+ and the mass-eigenstate quark fields U^i and D^j:

$$\frac{-i}{\sqrt{2}m_\psi}\,\Theta^{a+}\,\overline{U}^{\,i}T^a\Big[(C\,V_{\rm KM})_{ij}\,m_{d_j}P_R - m_{u_i}\left(C^\dagger\,V_{\rm KM}\right)_{ij}P_L\Big]\,D^j + \text{H.c.} \quad (3.7)$$

where $V_{\rm KM}$ is the CKM matrix, and m_{u_i}, m_{d_i} are the physical masses for the quarks of the ith generation. The 3×3 matrix C is given by

$$C = V^\dagger_{u_L}\,c\,V_{u_L} \quad , \quad (3.8)$$

where c is the matrix whose elements are given in Eq. (3.6), and V_{u_L} is the matrix that transforms the left-handed up-type quarks from the mass eigenstates to the gauge eigenstates, $u = V_{u_L}U$.

Based on interactions (3.7) we find that the width for the decay of the charged octo-triplet into a quark pair is

$$\Gamma(\Theta^+ \to c\,\bar{s}) \simeq \frac{m_c^2 + m_{\bar{s}}^2}{64\,\pi\,m_\psi^2}\,|C_{22}|^2 M_\Theta \ , \quad (3.9)$$

where we have omitted $\mathcal{O}(m_q^4)$ terms and off-diagonal CKM elements, and have not included QCD corrections. Taking the charm quark mass $m_c = 1.3$ GeV gives

$$\Gamma(\Theta^+ \to c\,\bar{s}) \simeq 1.3\times 10^{-6}\,\text{GeV}\,|C_{22}|^2 \times \frac{M_\Theta}{150\,\text{GeV}}\left(\frac{1\,\text{TeV}}{m_\psi}\right)^2 . \quad (3.10)$$

Compared with the decay into Wg computed in Eq. (2.12), the above Θ^+ decay into a pair of jets can easily dominate. For example, for $M_\Theta = 150$ GeV, $\mu_\Theta = 1$ GeV, $C_{22} = 0.1$, and $m_\psi = 1.1$ TeV, we find $\Gamma(\Theta^+ \to c\,\bar{s}) \simeq 3.7\,\Gamma(\Theta^+ \to W\,g)$.

The width for the decay into $c\,\bar{b}$ is sensitive to different C_{ij} parameters:

$$\frac{\Gamma(\Theta^+ \to c\,\bar{b})}{\Gamma(\Theta^+ \to c\,\bar{s})} \simeq \frac{1}{|C_{22}|^2}\left(\frac{m_b^2}{m_c^2}\,|C_{23}|^2 + |C_{32}|^2\right), \quad (3.11)$$

where $m_b \approx 4.2$ GeV is the b quark mass.

If $M_\Theta > m_t + m_b$, the decay involving a top quark opens up:

$$\Gamma(\Theta^+ \to t\bar{b}) \simeq 2.2\times 10^{-2}\,\text{GeV}\,|C_{33}|^2\left(1-\frac{m_t^2}{M_\Theta^2}\right)^2 \times \frac{M_\Theta}{150\,\text{GeV}}\left(\frac{1\,\text{TeV}}{m_\psi}\right)^2 , \quad (3.12)$$

where we have set $m_t = 173$ GeV and ignored m_b^2 terms. Due to an m_t^2/m_c^2 enhancement compared to Eq. (3.9), this decay dominates unless $|C_{33}| < 10^{-2}|C_{22}|$. The decay $\Theta^+ \to t\bar{s}$ has the same width except for the $C_{33} \to C_{23}$ replacement.

Similar expressions give the 2-body widths for the neutral octo-triplet decaying to $c\bar{c}$, $b\bar{b}$, or top pairs if $M_\Theta > 2m_t$.

The m_t^2/m_c^2 enhancement in Eq. (3.12) is so large that even for $M_\Theta < m_t + m_b$ the 3-body decay through an off-shell top quark, $\Theta^+ \to W^+ b\,\bar{b}$, needs to be taken into account. Its width is

$$\Gamma(\Theta^+ \to W^+ b\bar{b}) = \frac{\alpha\,|C_{33}|^2\,m_t^4}{64\pi^2\sin^2\theta_W\,m_\psi^2}\mathcal{F}(M_\Theta) \ . \quad (3.13)$$

The the function $\mathcal{F}$, of mass dimension -1, is given by integrating the matrix element over phase space:

$$\mathcal{F}(M_\Theta) = \int_0^{E_0} d\overline{E}_{\bar{b}} \int_{E_0-\overline{E}_{\bar{b}}}^{E_b^{\rm max}} dE_b \, \frac{E_b + (E_0 - \overline{E}_{\bar{b}})\left[\frac{2M_\Theta}{M_W^2}(E_0 - E_b) - 1\right]}{(M_\Theta^2 - 2M_\Theta\overline{E}_{\bar{b}} - m_t^2 + m_b^2)^2 + m_t^2\Gamma_t^2} \ , \quad (3.14)$$

where E_0 is the maximum energy of the $\bar{b}$ or b jet,

$$E_0 = \frac{M_\Theta^2 - M_W^2}{2M_\Theta} \quad , \quad (3.15)$$

and $E_b^{\rm max}$ is the maximum b energy for a fixed $\bar{b}$ energy $\overline{E}_{\bar{b}}$,

$$E_b^{\rm max} = \frac{E_0 - \overline{E}_{\bar{b}}}{1 - 2\overline{E}_{\bar{b}}/M_\Theta} \quad . \tag{3.16}$$

In Eq. (3.14) we neglected m_b everywhere (which is a good approximation for $m_b^2 \ll E_0^2$) with the exception of the denominator where the m_b^2 term becomes important for M_Θ near the 2-body threshold, $m_t + m_b$. To cover that case we also included the top quark width, $\Gamma_t \approx 1.3$ GeV, in the propagator. Numerically, the 3-body width can be written as

$$\Gamma(\Theta^+ \to W^+ b\bar{b}) \;\simeq\; 2.9\times 10^{-6}\,{\rm GeV}\,|C_{33}|^2 \times \frac{\mathcal{F}(M_\Theta)}{\mathcal{F}(150\ {\rm GeV})}\left(\frac{1\,{\rm TeV}}{m_\psi}\right)^2 . \tag{3.17}$$

The ratio $\mathcal{F}(M_\Theta)/\mathcal{F}(150\ {\rm GeV})$ is given by 1.51 for $M_\Theta = 155$ GeV, and by 2.28 for $M_\Theta = 160$ GeV.

It is remarkable that the above 3-body decay through a virtual top quark has a width close to that for the 2-body decay into $c\bar{s}$, given in Eq. (3.10). Assuming for illustration that $|C_{23}|, |C_{32}| \ll |C_{22}| = |C_{33}|$ we find that the branching fraction into $Wb\bar{b}$ is 69, 76, 82% for $M_\Theta = 150, 155, 160$ GeV, respectively.

Finally, the decay $\Theta^+ \to W b\bar{s}$, of width

$$\Gamma(\Theta^+ \to W^+ b\bar{s}) \approx \frac{|C_{23}|^2}{|C_{33}|^2}\,\Gamma(\Theta^+ \to W^+ b\bar{b}) \ , \tag{3.18}$$

may also have a substantial branching fraction if the C_{23} parameter is large. In that case, though, the main competing channel is likely to be $\Theta^+ \to c\,\bar{b}$, as can be seen from Eq. (3.11).

3.2 $B_s - \bar{B}_s$ mixing

Since Ψ has flavor-dependent couplings, its interactions can contribute to flavor-changing neutral processes. The largest couplings are to the 3rd and perhaps 2nd generation quarks, so that we expect that the most prominent effect is in $B_s - \overline{B}_s$ meson mixing. This proceeds through the tree-level diagram in Figure 4. Integrating out Θ and Ψ generates the effective four-Fermi operator

$$\mathcal{L}_{B_s-\overline{B}_s} = \left(\frac{C_{23}\,m_b}{2M_\Theta m_\psi}\right)^2 \left(\,\overline{b}_R\,T^a s_L\right)^2 + {\rm H.c.} \tag{3.19}$$

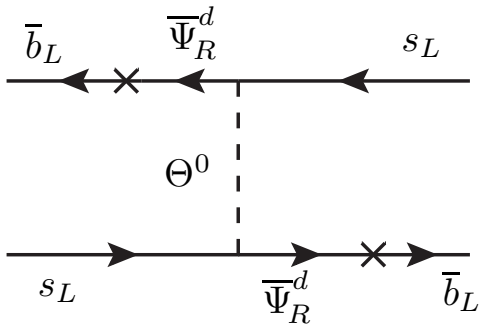

Figure 4: Leading contribution to $B_s - \overline{B}_s$ mixing through Ψ and Θ interactions. Other diagrams differ only by the placement of $\overline{\Psi}_R Q_L$ mass insertions, and are suppressed by additional powers of m_s.

Here we have used the fermion field equations and ignored terms suppressed by factors of m_s/m_b.

The matrix element of the Hamiltonian due to Θ^0 exchange is

$$\left\langle \overline{B}_s|\mathcal{H}_\Theta|B_s\right\rangle \simeq \left(\frac{C_{23}}{M_\Theta m_\psi}\right)^2 M_{B_s}^4 f_{B_s}^2 \eta_{\rm QCD}\,\frac{5B_2+3B_3}{288} \ , \tag{3.20}$$

where M_{B_s} and $f_{B_s} = (231\pm15)$ MeV [27] are the B_s meson mass and decay constant respectively; $\eta_{\rm QCD} \simeq 1.7$ is the QCD correction for the operator in Eq. (3.19) due to running from the scale M_Θ down to M_{B_s} [28]; $B_2 \simeq 0.80$ and $B_3 \simeq 0.93$ are lattice "bag" parameters [29] for the singlet-singlet and octet-octet color structures arising from operator (3.19), respectively.

It is convenient to parametrize the contribution to B_s mixing from Θ^0 relative to the standard model one as

$$\frac{\left\langle \overline{B}_s|\mathcal{H}_{\rm SM}+\mathcal{H}_\Theta|B_s\right\rangle}{\left\langle \overline{B}_s|\mathcal{H}_{\rm SM}|B_s\right\rangle} \equiv C_{B_s} e^{-i\phi_s} \ , \tag{3.21}$$

where C_{B_s} is a positive parameter and $-\pi < \phi_s < \pi$ is a phase. The standard model contribution can be extracted from the estimate given in [30, 31]:

$$\left\langle \overline{B}_s|\mathcal{H}_{\rm SM}|B_s\right\rangle \approx \left(8.0\times10^{-6}\ {\rm GeV}\right)^2 (1\pm0.15) \ . \tag{3.22}$$

The 15% theoretical uncertainty shown above loosens the constraint on C_{B_s} set by the measured B_s mass

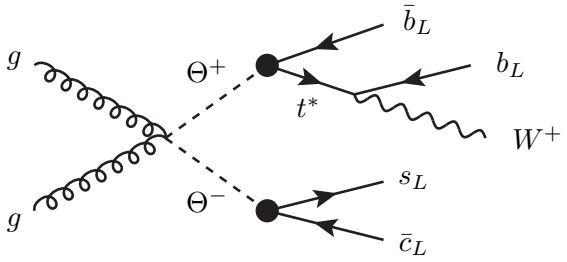

Figure 5: Representative diagram for pair production of charged octo-triplets through gluon fusion with a $(jj)(Wb\bar{b})$ final state. The $\bullet$ symbol denotes dimension-5 operators induced by the Ψ fermion. Similar diagrams lead to $4j$, $(W^+b\bar{b})(W^-b\bar{b})$,$(W^+b\bar{s})(jj)$, or $(jb)(Wb\bar{b})$ final states.

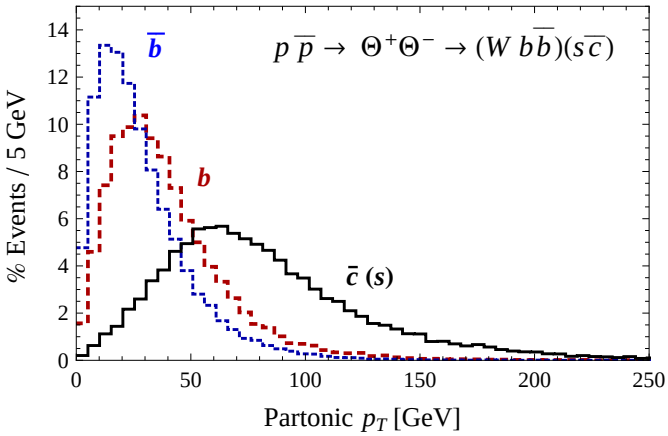

Figure 6: Partonic p_T distributions for the quarks arising from the $\Theta^+\Theta^- \to (c\bar{s})(W^-b\bar{b})$ process (see Figure 5) with $M_\Theta = 155$ GeV. The c or $\bar{s}$ distribution (black solid line) peaks at higher p_T and has a longer tail than the b and $\bar{b}$ distributions (blue dotted and red dashed lines).

difference: $C_{B_s} \approx 0.98 \pm 0.15$. Comparing Eqs. (3.20) and (3.21) we find

$$m_\psi \;=\; 1.1 \text{ TeV} \times |C_{23}| \left(\frac{150\,\text{GeV}}{M_\Theta}\right) \times \left(C_{B_s}^2 + 1 - 2C_{B_s}\cos\phi_s\right)^{-1/4} \;, \quad (3.23)$$

and a less illuminating expression of ϕ_s in terms of the phase of C_{23}. For $M_\Theta = 150$ GeV, $C_{23} = 0.2$, $C_{B_s} = 0.9$, and a small CP-violating phase $\phi_s = -5°$, we get $m_\psi = 568$ GeV. However, if the phase is large, as suggested by the D0 like-sign dimuon asymmetry [32], then m_ψ is below the electroweak scale; for example $\phi_s = -45°$ gives $m_\psi = 260$ GeV. Such a light vector-like quark is not ruled out. Note that the main decay mode is likely to be $\Psi^d \to \Theta^+\bar{c} \to (c\bar{s})\bar{c}$, so that Ψ pair production leads to a 6-jet final state. The CDF search [33] in a similar channel gives a lower limit on the $3j$ resonance mass below 200 GeV.

This model also contributes to $b \to s\gamma$ decays at the 1-loop level. Since these diagrams involve two mass insertions and suffer additional loop suppression, we expect their contributions to be small.

3.3 Dijet resonance plus a W boson at the Tevatron

Pair production of octo-triplets, through their QCD couplings to gluons, gives rather large cross sections at the Tevatron, as shown in Figure 2. In the presence of the vectorlike quark Ψ and assuming that the trilinear coupling μ_Θ is small enough (see section 3.1), the main decay modes of Θ^+ are into a pair of jets ($c\bar{b}$ or $c\bar{s}$) and into $Wb\bar{b}$ ($Wb\bar{s}$ is also possible, but at least one b quark is always present due to the decay through the off-shell top quark). One of the final states (see Figure 5) arising from $\Theta^+\Theta^-$ production is then $(jj)(Wb\bar{b})$, where j is any jet and the parantheses indicate a resonance at M_Θ. The branching fractions depend on the $|C_{22}|$ and $|C_{33}|$ parameters, and are also quite sensitive to M_Θ, as discussed at the end of section 3.1. We expect that next-to-leading order QCD corrections to this process, which affect both production and decays, increase the rate by a K factor in the $1 - 1.5$ range.

The two b jets arising from the decay through an off-shell top quark typically have energies below $(M_\Theta - M_W)/2 - m_b$, so are softer than those arising from the 2-body decay, which typically have energies around $M_\Theta/2$. Figure 6 shows the transverse momentum of each quark in the $(c\bar{s})(Wb\bar{b})$ final state for $M_\Theta = 155$ GeV, computed with MadGraph 5 [22] with model files generated by FeynRules [23]. Given that the quarks from the 2-body decay have the highest p_T, the invariant mass distribution of the two leading jets from the $p\bar{p} \to \Theta^+\Theta^- \to (jj)(Wb\bar{b})$ process exhibits a peak near M_Θ.

In order to compare this signal with the CDF dijet excess [16], we generate partonic events using

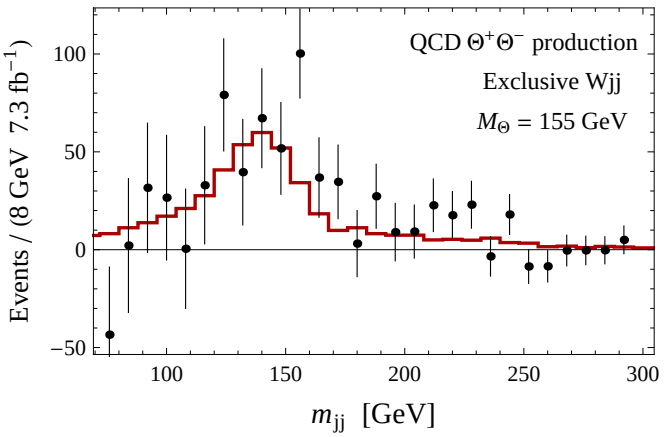

Figure 7: Invariant mass distribution for the leading two jets arising from the $\Theta^+\Theta^- \to (jj)(Wb\bar{b}) \to \ell\nu + 4j$ process, where $\ell = e, \mu$, at the Tevatron with exactly 2 jets passing the cuts. The red solid line represents events in our simulation for $\mathcal{B}(\Theta^\pm \to W^\pm b\bar{b}) = 40\%$ and $M_\Theta = 155$ GeV. The data points with 1σ statistical error bars are taken from the CDF excess region (Fig. 2 of [15]) after the background (including WW/WZ) has been subtracted, with the normalization of the CDF Wjj background increased by 1%.

MadGraph 5 for the $p\bar{p} \to \Theta^+\Theta^- \to (jj)(Wb\bar{b})$ process with $W \to e\nu, \mu\nu, \tau\nu$. We then use PYTHIA 6.4 [34] for hadronization and parton showering, and PGS 4 [35] for detector-level effects. We impose[2] the same cuts as CDF [16]: lepton $p_T^\ell > 20$ GeV and $|\eta^\ell| < 1$, missing transverse energy $\not{E}_T > 25$ GeV, transverse W mass $M_T(W) > 30$ GeV, jet $p_T^j > 30$ GeV and $|\eta^j| < 2.4$, separation between jets $|\Delta\eta_{jj}| < 2.5$, azimuthal separation between the missing E_T and the leading jet $|\Delta\phi| > 0.4$, and $p_{Tjj} \geq 40$ GeV for the leading dijet system. The resulting dijet invariant mass (m_{jj}) distribution for events with exactly 2 jets is shown in Figure 7 (solid red line) for $M_\Theta = 155$ GeV and a branching fraction $\mathcal{B}_3 \equiv \mathcal{B}(\Theta^+ \to W^+ b\bar{b}) = 40\%$. The rate for this process (before cuts and without including the $W \to \ell\nu$ branching fraction) is

$$2\mathcal{B}_3(1-\mathcal{B}_3)\,\sigma\big(p\bar{p} \to \Theta^+\Theta^-\big) \simeq 3.2 \text{ pb}\,, \quad (3.24)$$

where the factor of 2 takes into account the charge conjugated process with a W^- in the final state. The acceptance of the cuts is 6.2%, so that in 7.3 fb^{-1} of data there are about 470 Wjj events due to $\Theta^+\Theta^-$ production. The high-mass tail of the m_{jj} distribution is mainly due to events in which the two hardest jets come from different octo-triplets.

To compare our simulated m_{jj} with the CDF data shown in Figure 2 (left-side plot) of [15] we need to subtract all standard model background. The CDF Collaboration has fitted the normalization of the large CDF Wjj background to the data assuming a Gaussian shape for the signal. In the presence of the wider shape arising from our $\Theta^+\Theta^-$ signal the Wjj background normalization is likely to change; increasing it by 1% gives a reasonable agreement between our m_{jj} and the CDF data after background subtraction (Figure 7).

If the K factor accounting for the QCD corrections is significantly larger than 1.0, then $\mathcal{B}_3$ should be decreased while keeping the rate in Eq. (3.24) fixed. The highest data point, in the $152 - 160$ GeV bin could indicate that M_Θ values larger than 155 GeV are preferred. However, the jet reconstruction performed by our PGS simulation is likely to be less efficient than the CDF reconstruction, so that a larger fraction of the hadrons is missed, reducing the jet energy. Thus, the dijet mass distribution in Figure 7 is likely to be artificially shifted to lower m_{jj} compared to the data, implying that masses even below 155 GeV may be acceptable. For $M_\Theta = 150$ GeV the cross section is larger by a factor of 1.24, so that an acceptable fit is obtained for a smaller $\mathcal{B}_3 \approx 26\%$.

The D0 search [17] in the same channel with 4.3 fb^{-1} has ruled out a 1.9 pb signal at the 95% confidence level, based on the assumptions that the dijet resonance X has a Gaussian shape with a width of 15.7 GeV and is produced like the Higgs boson, $p\bar{p} \to W^* \to WX$, through a virtual W. Clearly, neither of these assumptions applies to our explanation for the CDF excess. The shape of our dijet invariant mass distribution is quite different than a Gaussian: it has a high tail below the peak due to final state radiation, and it has a long tail above the peak due to the two additional jets from Θ decay. The different shape is important because the fit of the background plus signal could improve significantly in the presence of our flatter signal shape compared to the pointy Gaussian. The production through $\Theta^+\Theta^-$ is also very different than through WX, and leads to a different acceptance. Hence, the D0 result cannot rule out our Wjj signal.

[2] We impose cuts on the PGS output using a modified version of the Chameleon package [36].

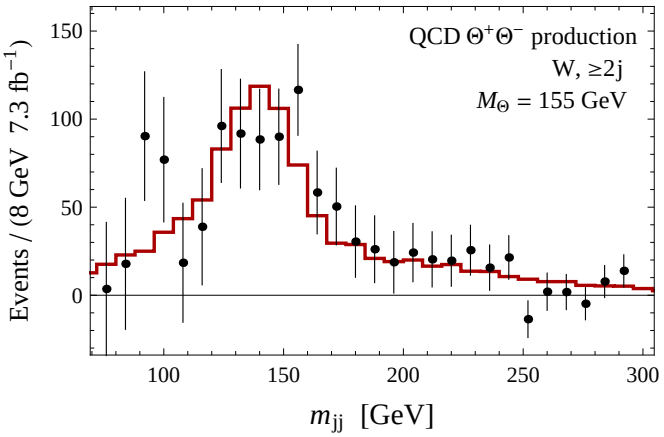

Figure 8: Same as Figure 7 except that two or more jets pass the cuts. The data points with error bars are taken from the CDF excess region (Fig. 5 of [15]) after background subtraction with the CDF Wjj background normalization reduced by 3%.

The requirement in the exclusive Wjj search [16] that exactly two jets pass the cuts rejects events arising from $\Theta^+\Theta^-$ production where one of the b jets has $p_T^j > 30$ GeV. These events, however, show up in the inclusive Wjj search (Fig. 5 of [15]) where two or more jets pass the cuts. The normalization of the large Wjj background is fitted to the data independently in the exclusive and inclusive cases. The additional events mentioned above require the normalization of the CDF inclusive Wjj background to be reduced. Figure 8 shows that the QCD production of $\Theta^+\Theta^-$ gives a $W + n$ jet signal with $n \geq 2$ that is consistent with the CDF data when the normalization of the CDF inclusive Wjj background is reduced by 3%.

There are a few experimental tests of this interpretation of the CDF excess. Even though the two b jets are relatively soft, the fraction of events that have a 3rd jet that passes all the cuts is large enough to allow the b tagging of the 3rd hardest jet. Furthermore, the additional two b jets allow the reconstruction of the full event. One complication here is that there is a large background from semileptonic $t\bar{t}$ events. Nevertheless, the signal has the property that the reconstructed W boson together with the two b jets form an invariant mass peak at M_Θ, so that it can be separated from the background.

Another test is the process where both octo-triplets decay through an off-shell t quark, $p\bar{p} \to \Theta^+\Theta^- \to (W^+b\bar{b})(W^-b\bar{b})$. The rate for this is smaller

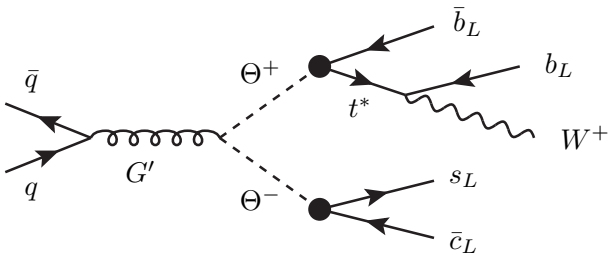

Figure 9: Same as Figure 5 except the pair of octo-triplets is resonantly produced through an s-channel coloron.

by a factor of $2(1/\mathcal{B}_3 - 1) \approx 3$ than for the $(jj)(Wb\bar{b})$ signal. Although this signal also suffers from a large $t\bar{t}$ background, it may be observable due to its relatively large rate of ~ 1 pb at the Tevatron.

Given that the W boson in the $(jj)(Wb\bar{b})$ signal originates from a decay through an off-shell top quark, there is no similar signal involving a Z boson or a photon.

The process $\Theta^+\Theta^- \to (Wb\bar{b})(jj)$ may affect measurements of the $t\bar{t}$ cross section. However, these measurements often rely on algorithms trained specifically to find top pairs and are, thus, less sensitive to new particles that decay into similar final states. Tevatron measurements involving b-tags [37] may be sensitive to octo-triplet decays, but their W-plus-jets background normalization is fitted to the data so that they do not necessarily constrain octo-triplet decays. Furthermore, b-tagging efficiency decreases for softer jets such as our b and $\bar{b}$ (see Figure 6).

Nevertheless, there are some measurements without neural networks or b-tags of the $t\bar{t}$ cross section in the lepton-plus-jets channel at the LHC [38], so these constraints must be checked more carefully. Simulating octo-triplet production with MadGraph, Pythia, and PGS and imposing cuts from both the ATLAS and CMS collaborations [38], we find that, for $\mathcal{B}_3 = 40\%$ and $M_\Theta = 155$ GeV, the octo-triplet contribution to events with 3 or more jets is within the statistical error bars at 95% confidence. This approach is conservative and takes the ATLAS and CMS background simulations and extracted $t\bar{t}$ signal at face value; since these measurements are not dedicated new-physics searches, potential octo-triplet decays would be bundled with the $t\bar{t}$ signal, which would make the statistical bound unrealistically constraining.

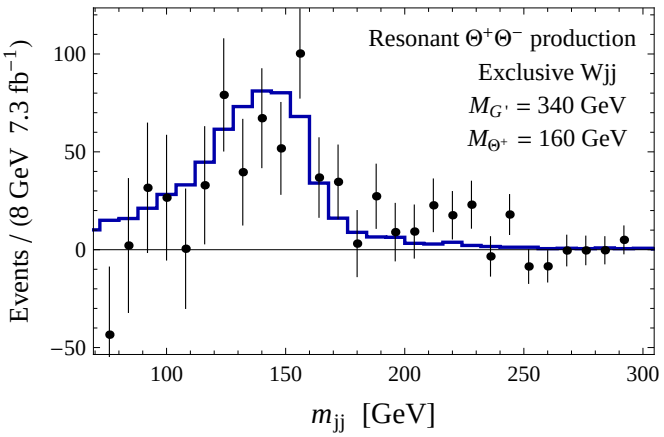

Figure 10: Same as Figure 7 except that a coloron contributes in the s-channel to $\Theta^+\Theta^-$ production. The blue solid line represents events in our simulation for $\mathcal{B}(\Theta^\pm \to W^\pm b\bar{b}) = 3.9\%$, $M_{\Theta^+} = 160$ GeV, $M_{G'} = 340$ GeV, $\tan\theta = 0.15$ and $\Gamma_{G'} = 6.5$ GeV.

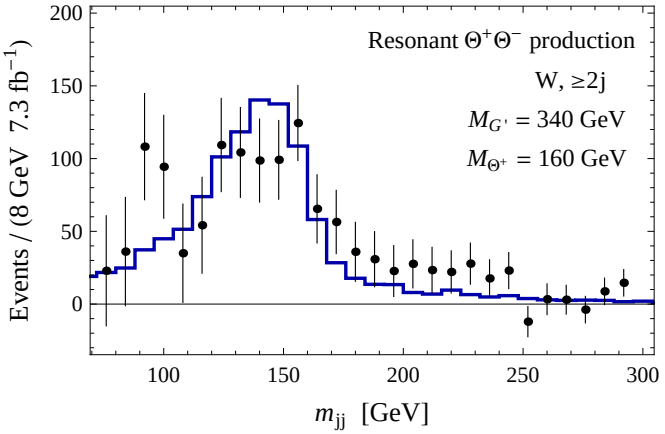

Figure 11: Same as Figure 10 except that two or more jets pass the cuts. The CDF data points are taken from Fig. 5 of [15] after background subtraction with the normalization of the CDF Wjj background reduced by 5%.

3.4 Resonant production of $\Theta^+\Theta^-$

A mass near 150 GeV also appears in another deviation from the standard model: preliminary CDF data in the $3b$ final state shows an excess in the invariant mass distribution of the leading two jets [4]. That deviation may arise from the $\Theta^0\Theta^0 \to (b\bar{b})(b\bar{b})$ process [3]. The transverse energy distributions of the jets in that case appear to favor a pair production mechanism through an s-channel resonance rather than through QCD. The simple renormalizable coloron model presented in [3] can be easily adapted to include the octo-triplet discussed here. It is sufficient to charge the scalar field Σ (responsible for breaking the $SU(3) \times SU(3)$ extension of the QCD gauge group [39]) under $SU(2) \times U(1)_Y$, as proposed in [40]. The color-octet scalars present in the spectrum can be identified with our $\Theta^\pm$ and Θ^0 (although a small mass splitting can be induced by the Higgs VEV), and they couple to the coloron field G'_μ as follows

$$g_s \frac{1-\tan^2\theta}{2\tan\theta} f^{abc} G'^a_\mu \Big[\Big(\Theta^{b+} \partial^\mu \Theta^{c-} + \text{H.c.} \Big) + \Theta^{b0} \partial^\mu \Theta^{c0} \Big] \quad . \qquad (3.25)$$

Here $\tan\theta$ is a parameter in the $0.1 - 0.3$ range. The coloron couples to quarks proportional to $g_s \tan\theta$, while it couples only in pairs to gluons at renormalizable level [2]. Thus, single G'_μ production proceeds entirely through quark-antiquark collisions.

The resonant $p\bar{p} \to G'_\mu \to \Theta^+\Theta^-$ production (Figure 9) may be an order of magnitude larger than QCD pair production [3]. This theory preserves the good agreement with the CDF data shown in Figure 7 provided the branching fraction $\mathcal{B}_3$ is decreased accordingly. The width of the coloron $\Gamma_{G'}$ is sensitive to $\tan\theta$ and to the octet masses. Assuming that the coloron decays only into $q\bar{q}$, $\Theta^+\Theta^-$ and $\Theta^0\Theta^0$ (additional decay channels may increase the width [3]), we find $\Gamma_{G'}$ in the $3.2 - 6.5$ GeV range for $M_{\Theta^+} = 160$ GeV, $\tan\theta = 0.15$, a coloron mass $M_{G'} = 340$ GeV, and M_{Θ^0} in the $160 - 140$ GeV range. For this set of parameters with $\Gamma_{G'} = 6.5$ GeV we generate events as described in section 3.3. The invariant mass distribution of the leading two jets is shown in Figure 10 for a rate

$$2\mathcal{B}_3(1-\mathcal{B}_3)\,\sigma\big(p\bar{p} \to G' \to \Theta^+\Theta^-\big) \simeq 3.8 \text{ pb} \; . \qquad (3.26)$$

Acceptance (without including W branching fractions) is 7.3% for this process. The branching fraction inferred from the above rate is small, $\mathcal{B}_3 = 3.9\%$, implying that the coloron $\Theta^+\Theta^-$ production dominates by an order of magnitude over the QCD $\Theta^+\Theta^-$ contribution. Nevertheless, we include in Figure 10 both production mechanisms and their interference, as well as the electroweak $\Theta^+\Theta^-$ production.

Figure 11 shows the m_{jj} distribution in the inclusive case (W plus two or more jets), with the normalization of the CDF Wjj background reduced by 5%. The subtracted data is consistently higher

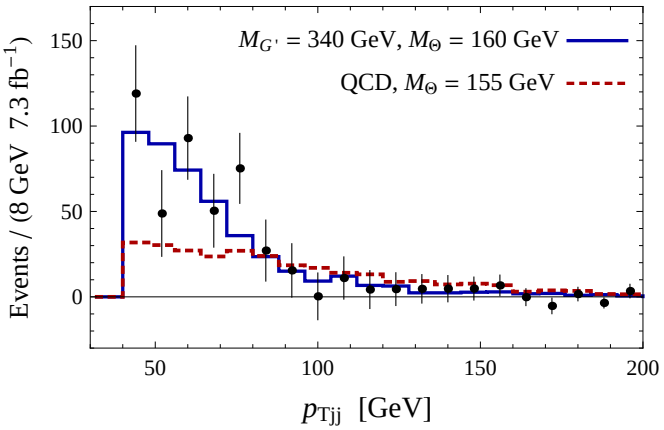

Figure 12: p_T distribution of the dijet system for events satisfying 115 GeV $\leq m_{jj} \leq$ 175 GeV. The blue solid line is for a coloron with the same parameters as in Figure 10, while the red dashed line is for QCD $\Theta^+\Theta^-$ production with $M_{\Theta^+} = 155$ GeV. The CDF data points with statistical error bars are taken from Fig. K9 of [41] after background subtraction consistent with Fig. 7.

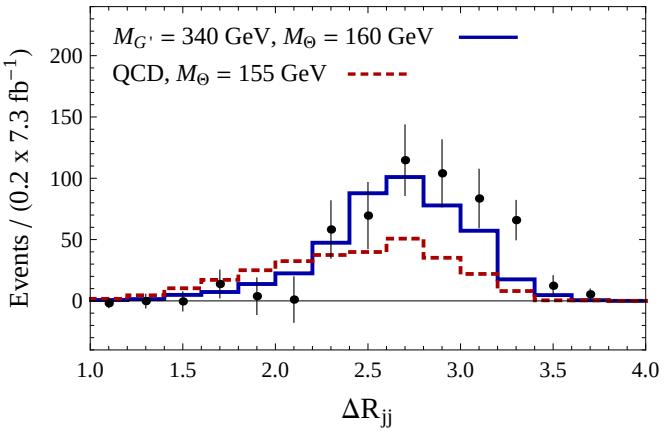

Figure 13: Same as Figure 12 for the angular separation ΔR_{jj} of the two leading jets (CDF data taken from Fig. K7 of [41]).

than the signal in the $m_{jj} \approx 170-240$ GeV range, so one could conclude that the QCD production mechanism (see Figure 8) provides a better description of the CDF data. However, next-to-leading order effects are not included in these figures, and it is conceivable that they sufficiently raise the high-mass tail of the resonant production shown in Figure 11. Furthermore, the CDF result for the inclusive case (Fig. 5 of [15]) does not include systematic errors. We also emphasize that our detector simulation using PGS 4 [35] is only a rough approximation to the CDF full detector simulation.

A better discriminant between the resonant and QCD production mechanisms is provided by the CDF kinematic distributions [41] for the exclusive search in the $m_{jj} \approx 115 - 175$ GeV window. The transverse momentum distribution of the dijet system (Figure 12) shows that resonant production fits the data much better than QCD $\Theta^+\Theta^-$ production. We reach the same conclusion using the ΔR_{jj} distribution of the angular separation between the two jets (Figure 13). Although some of the data points are not well fitted (the $p_{Tjj} = 72 - 80$ GeV bin and the $\Delta R_{jj} = 3.2 - 3.4$ bin) by our theoretical predictions, the shapes of both the p_{Tjj} and ΔR_{jj} distributions are in remarkable agreement. In both Figures 12 and 13 we use the same background subtraction as in Figure 7, where only one background (Wjj with combined electron and muon contributions) is rescaled (increased by 1%). We expect that a fit of the standard model background plus our signal, where various background normalizations are allowed to vary, would improve the agreement between $\Theta^+\Theta^-$ production and the CDF Wjj excess.

3.5 LHC Signals

QCD $\Theta^+\Theta^-$ production, which proceeds through gluon-gluon collisions, is two orders of magnitude larger at the 7 TeV LHC than at the Tevatron (see Figure 2), so that the $(jj)(Wb\bar{b})$ signal discussed in section 3.3 will soon be within the reach of the CMS and ATLAS experiments. Using typical parameters that explain the CDF dijet resonance, $\mathcal{B}_3 = 40\%$ and $M_\Theta = 155$ GeV, we find that the process in Figure 5 has a leading-order rate (before cuts) of

$$\sigma\big(pp \to \Theta^+\Theta^- \to (jj)(\ell\nu b\bar{b})\big) \simeq 52 \text{ pb} \quad , \quad (3.27)$$

where $\ell = e, \mu$. Furthermore, the $(W^+b\bar{b})(W^-b\bar{b})$ process also has a large rate, suppressed only by a factor of $2(1/B_3 - 1) \approx 3$ compared to $(jj)(Wb\bar{b})$, so the fully leptonic $(\ell^+\nu b\bar{b})(\ell^-\bar{\nu}b\bar{b})$ signal has a cross section of 3.7 pb and will also be soon within the reach of the LHC.

In the non-minimal model (section 3.4 and Figure 9) where resonant $G'_\mu \to \Theta^+\Theta^-$ production is the main process responsible for the CDF excess, the $(jj)(\ell\nu b\bar{b})$ rate at the 7 TeV LHC is reduced by a

factor of ~ 5 compared to Eq. (3.27), due to smaller parton distributions for quark-antiquark collissions:

$$\sigma\big(pp \to G' \to \Theta^+\Theta^- \to (jj)(\ell\nu b\bar{b})\big) \simeq 10 \text{ pb} \ . \quad (3.28)$$

Although QCD $\Theta^+\Theta^-$ production is still present in the coloron model, explaining the CDF signal requires a 10 times smaller $\mathcal{B}_3$ branching fraction, which reduces the gluon initiated contribution to the $(jj)(Wb\bar{b})$ signal. The smaller $\mathcal{B}_3 \approx 3.9\%$ also suppresses the $(W^+b\bar{b})(W^-b\bar{b})$ signal in this model (the rate is 43 fb).

While our analysis has emphasized the region around $M_\Theta = 150$ GeV, future searches could discover much heavier octo-triplets which decay into final states involving top quarks. For non-negligible values of the C_{33} parameter, the processes $\Theta^+\Theta^- \to (t\bar{b})(\bar{t}b)$ and $\Theta^0\Theta^0 \to 4t$ are important tests of the octo-triplet decaying through higher-dimensional operators (these final states have been studied in [14]).

4 Conclusions

We have shown that the renormalizable extension of the standard model with one octo-triplet (*i.e.*, a scalar in the adjoint representation of the standard model gauge group) involves two new parameters: the octo-triplet mass M_Θ and cubic self-coupling μ_Θ. For $\mu_\Theta^2/M_\Theta \gg 10^{-9}$ GeV the charged octo-triplet almost always decays into Wg in the absence of other new particles. The rate for this 1-loop process is accidentally suppressed (see Appendix C), but the decay is prompt as long as $\mu_\Theta^2/M_\Theta \gtrsim 10^{-7}$ GeV. The neutral octo-triplet decays to Zg or γg, with widths comparable to that for $\Theta^\pm \to W^\pm g$. For $\mu_\Theta \to 0$, the main decay is a tree-level 3-body process, $\Theta^\pm \to \Theta^0 e^\pm \nu$, with a displaced vertex, while Θ^0 is stable.

At the Tevatron and the LHC, octo-triplets are produced in pairs with relatively large cross sections (see Figure 2). The main signatures are

$$\begin{aligned} &\Theta^+\Theta^- \to (W^+g)(W^-g) \ , \quad (4.1)\\ &\Theta^0\Theta^0 \to (Zg)(Zg) \ , \ (Zg)(\gamma g) \ , \ (\gamma g)(\gamma g) \ . \end{aligned}$$

The rates for these processes suggest that Tevatron experiments can be sensitive to M_Θ up to a few hundred GeV, and LHC experiments to M_Θ above 1 TeV; however, more precise sensitivity estimates require detailed studies of the backgrounds.

Since octo-triplets have very small widths, decays through higher-dimensional operators may compete with the 1-loop processes. Operators of the type $\Theta\overline{Q}\not{\partial}Q$ may be induced by a heavy vectorlike quark, and lead to the $\Theta^+ \to t\bar{b}$ decay for $M_\Theta \gtrsim 175$ GeV. For a lighter octo-triplet, there is competition between the 2-body decays $\Theta^+ \to c\bar{s}$ or $c\bar{b}$ and the 3-body decays $\Theta^+ \to t^*\bar{b} \to Wb\bar{b}$ or $t^*\bar{s} \to Wb\bar{s}$ through an off-shell top quark. The neutral octo-triplet decays mainly to $b\bar{b}$, $c\bar{c}$, $W^+b\bar{c}$ and $W^-\bar{b}c$ for $M_\Theta \lesssim m_t + m_c$, to $t\bar{c}$ and $\bar{t}c$ for larger masses below $2m_t$, and to $t\bar{t}$ for masses above $2m_t$. For a range of parameters, the branching fractions for these decays are larger than the ones into a gluon plus an electroweak boson mentioned above. The collider signatures for $M_\Theta \lesssim 175$ GeV then include

$$\begin{aligned} \Theta^+\Theta^- \to\ & (jc)(Wb\bar{b}) \ , \ (bc)(Wb\bar{b}) \ , \ (W^+b\bar{b})(W^-b\bar{b}) \ , \\ & (jc)(j\bar{c}) \ , \ (jb)(j\bar{b}) \ , \ \dots \ , \\ \Theta^0\Theta^0 \to\ & (b\bar{b})(b\bar{b}) \ , \ (b\bar{b})(c\bar{c}) \ , \ (b\bar{b})(Wbc) \ , \ \dots \ , \quad (4.2) \end{aligned}$$

For a heavier octo-triplet the signatures are mainly $(t\bar{b})(\bar{t}b)$ and $(t\bar{c})(\bar{t}c)$, while above 350 GeV the $4t$ final state also opens up.

Signatures of pair production followed by one octo-triplet decaying through higher-dimensional operators and the other decaying into a gluon and an electroweak gauge boson at one loop are also possible. These include $\Theta^+\Theta^- \to (Wg)(jc)$, $\Theta^0\Theta^0 \to (Zg)(c\bar{c})$ or $(\gamma g)(c\bar{c})$ and similar processes involving b quarks (or t quarks if kinematically allowed).

Some of the final states mentioned above, namely $(jc)(Wb\bar{b})$, $(jc)(Wbj)$, $(jc)(Wg)$, may be relevant to the CDF excess [16] in the dijet resonance plus W search. In the case where Θ^+ decays mostly into $c\bar{s}$ and $W^+b\bar{b}$, so that the process is $p\bar{p} \to \Theta^+\Theta^- \to (cj)(Wb\bar{b})$, we have shown that the b jets are substantially softer than the jets originating from the $\Theta^+ \to c\bar{s}$ decay. Events where these b jets do not pass the CDF cuts could explain the dijet resonance plus W signal if Θ has a mass in the $150 - 170$ GeV range.

We have compared two production mechanisms of charged octo-triplet pairs: through the QCD couplings to gluons (these are always present due to gauge invariance), and through an s-channel resonance (we have focused on a coloron, but a Z' coupled to octo-triplets would not be very different). Both mechanisms are consistent with the CDF excess in the dijet invariant mass distribution when

exactly two jets are required to pass the cuts. In the inclusive case (two or more jets pass the cuts), QCD $\Theta^+\Theta^-$ production fits the CDF data more precisely than resonant production. However, this difference is not conclusive given that the low tail of the resonant production compared to the background-subtracted data may be due to systematic errors in the standard model background, and may also be corrected by a fit of the background (with several free normalizations, as usual) plus coloron signal. Other kinematic distributions obtained by CDF [41] can differentiate various models more effectively. We have shown that the shapes of the transverse momentum distribution for the dijet system (p_{Tjj}) and of the angular separation distribution for the two leading jets (ΔR_{jj}) agree rather well with the resonant mechanism while being quite different than the predictions of QCD $\Theta^+\Theta^-$ production.

It is intriguing that almost the same mass (~ 150 GeV) appears in another deviation from the standard model, namely the $3b$ CDF search [4], which could be attributed to the $\Theta^0\Theta^0 \to (b\bar{b})(b\bar{b})$ process [3]. Resonant production through a coloron also agrees better to various kinematic distributions in that case.

The interpretation of the dijet plus W signal in terms of an octo-triplet decaying via an off-shell top quark can be tested by the b-tagging of the third jet, or by the reconstruction of the $Wb\bar{b}$ peak at the same mass as the dijet peak.

At the 7 TeV LHC, if octo-triplet production is through the QCD couplings to gluons, then the dijet-plus-W signal has a large cross section (52 pb for $M_{\Theta^+} = 155$ GeV) because it is dominated by gluon fusion. In the case of dominant production through an s-channel resonance coupled to $q\bar{q}$ like the coloron, the LHC signal is reduced to ~ 10 pb.

If the couplings of the vectorlike quark are complex, then tree-level Θ^0 exchange induces CP violation in $B_s - \bar{B}_s$ mixing. For a vectorlike quark mass of a few hundred GeV (which is allowed because its main decay is into three jets), this effect can be large enough to produce a significant part of the like-sign dimuon asymmetry observed by the D0 Collaboration [32].

We note that similar final states can also arise from a fermiophobic octo-doublet field. However, this has nontrivial couplings to the standard model Higgs doublet, so the mass splitting between charged and neutral components may be large. By contrast, the tiny mass splitting between charged and neutral octo-triplets suppresses the tree-level 3-body decays. Furthermore, the neutral octo-doublet decays into gluons, while $SU(2)_W$ symmetry forbids pure gluonic decays of the neutral octo-triplet.

Acknowledgments: We would like to thank Johan Alwall, Alberto Annovi, Yang Bai, William Bardeen, Chris Bouchard, Patrick Fox, Walter Giele, Roni Harnik, David E. Kaplan, Joachim Kopp, Adam Martin, Olivier Mattelaer, Yuhsin Tsai, and Ciaran Williams for helpful discussions and comments. GZK is supported by a Fermilab Fellowship in Theoretical Physics. Fermilab is operated by Fermi Research Alliance, LLC, under Contract DE-AC02-07-CH11359 with the US Department of Energy.

Appendix A: Feynman rules

The Feynman rules for octo-triplets, derived from Eqs. (2.1)-(2.5), are given by:

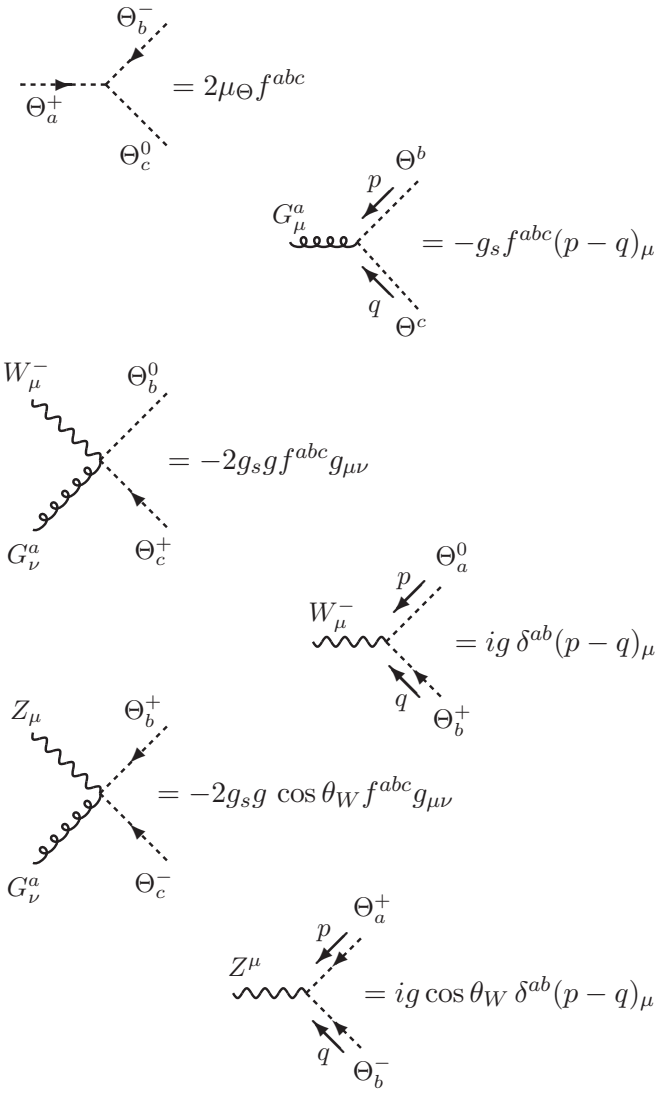

The Feynman rules involving photons are identical to those involving a Z boson shown above but with the replacement $g\cos\theta_W \to e$.

Appendix B: Tree-level octo-triplet decay

In this appendix we compute width for the 3-body decay of the charged octo-triplet through an off-shell W, as shown in Figure 14. We define p_e, p_ν, and p_0 to be the outgoing momenta for e, ν and Θ^0 respectively. Using the Feynman rule from Appendix A,

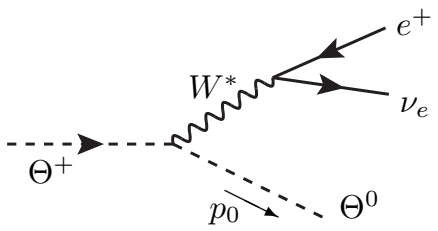

Figure 14: 3-body decay of the charged octo-triplet scalar through an off-shell W boson.

the amplitude for this process is

$$\mathcal{M} \simeq \frac{\sqrt{2}\,g^2}{M_W^2 - 2p_e{\cdot}p_\nu}\,\overline{u}(p_e)\,\not{p}_0 P_L v(p_\nu) \quad , \qquad \text{(B.1)}$$

where we have used the e, ν equations of motion in the massless lepton limit. Squaring the amplitude and summing over helicities we find

$$\overline{|\mathcal{M}|^2} = 4g^4\,\frac{2(p_e{\cdot}p_0)(p_\nu{\cdot}p_0) - p_e{\cdot}p_\nu M_{\Theta^0}^2}{(M_W^2 - 2p_e{\cdot}p_\nu)^2} \quad . \qquad \text{(B.2)}$$

The decay width in the Θ^+ rest frame is then given by

$$\Gamma(\Theta^+ \to \Theta^0 e^+ \nu) = \frac{g^4 M_{\Theta^+}}{16\pi^3}\int_0^\varepsilon dE_\nu \int_{\varepsilon - E_\nu}^{E_e^{\max}} dE_e \times \frac{M_{\Theta^+}(\varepsilon - E_\nu - E_e) + 2E_\nu E_e}{\left[M_W^2 - 2M_{\Theta^+}(\varepsilon - E_\nu - E_e)\right]^2} \quad , \qquad \text{(B.3)}$$

where ε is the maximum lepton energy,

$$\varepsilon = \frac{M_{\Theta^+}^2 - M_{\Theta^0}^2}{2M_{\Theta^+}} \quad , \qquad \text{(B.4)}$$

and $E_e^{\max}$ is the maximum positron energy for a fixed neutrino energy E_ν,

$$E_e^{\max} = \frac{\varepsilon - E_\nu}{1 - 2E_\nu/M_{\Theta^+}} \quad . \qquad \text{(B.5)}$$

The integrals in Eq. (B.3) can be performed analytically, with the result

$$\Gamma(\Theta^+ \to \Theta^0 e^+ \nu) = \frac{\alpha^2 M_W^4}{16\pi \sin^4\theta_W M_{\Theta^+}^3}\,\mathcal{G}\left(\frac{\varepsilon}{M_{\Theta^+}}, \frac{2M_{\Theta^+}^2}{M_W^2}\right) \qquad \text{(B.6)}$$

where we introduced a function

$$\mathcal{G}(x,r) = -\xi\,(1+r-rx)\ln\left(1-x+rx^2+\xi x\right) - \frac{1}{2}\left[\left(\frac{1}{2}-x\right)r^2+\xi^2-\xi\,(1+r-rx)\right]\ln(1-2x) + \frac{r^3x^3}{3}+\frac{3}{2}r^2x\,(1-x)+rx \quad , \tag{B.7}$$

with

$$\xi \equiv \xi\,(x,r) = \left[2r+(1-rx)^2\right]^{1/2} \quad . \tag{B.8}$$

Interestingly, the expansion of $r^{-4}\mathcal{G}(x,r)$ for $|x|<1$ starts at x^5, and the leading r-dependent term arises even later, at x^7:

$$\mathcal{G}(x,r) = \frac{r^4x^5}{15}\left[1+x+\frac{2}{7}\,(4-r)\,x^2\right]+O\left(x^8\right). \tag{B.9}$$

Translating this expansion into a power series in $\delta M \equiv M_{\Theta^+} - M_{\Theta^0}$ we find that the exact tree-level width of Eq. (B.6) is given, up to corrections of order $(\delta M)^8$, by

$$\Gamma(\Theta^+\to\Theta^0 e^+\nu) \simeq \frac{\alpha^2\,(\delta M)^5}{15\pi\sin^4\theta_W M_W^4}\left[1-\frac{3(\delta M)}{2M_{\Theta^+}} + \frac{4}{7}\left(\frac{9}{8}-\frac{M_{\Theta^+}^2}{M_W^2}\right)\left(\frac{\delta M}{M_{\Theta^+}}\right)^2\right]. \tag{B.10}$$

Appendix C: One-loop decay of a scalar octet into gauge bosons

In this Appendix we compute the width for a color-octet scalar decaying to a gluon and a (massive or massless) vector boson V_μ, which proceeds through scalar 1-loop diagrams like those of Figure 1. In particular, this computation applies to the process $\Theta^\pm \to W^\pm g$, $\Theta^0 \to \gamma g$ or Zg.

We label the V_μ and gluon 4-momenta (polarizations) by p_1 (ϵ_1) and p_2 (ϵ_2), respectively. Since the gluon is always transversely polarized ($\epsilon_2\cdot p_2 = 0$), angular momentum conservation demands that the other vector also be transverse, so $\epsilon_1\cdot p_1 = 0$. Given that the contraction $\epsilon_{\mu\nu\rho\sigma}\,p_1^\mu\epsilon_1^\nu\,p_2^\rho\,\epsilon_2^\sigma$, cannot arise from scalar triangle diagrams, the amplitude contains only two terms: $\epsilon_1\cdot\epsilon_2$ and $(\epsilon_1\cdot p_2)\,(\epsilon_2\cdot p_1)$. Furthermore, by the Ward-Takahashi identity the amplitude vanishes upon replacing ϵ_2 with p_2, so that the most general amplitude due to scalar loops is given by

$$\mathcal{M} = \frac{\mu_\Theta g_s\tilde{g}}{\pi^2}\,\mathcal{C}\left(\frac{1}{2}\,\epsilon_1\cdot\epsilon_2 - \frac{(\epsilon_1\cdot p_2)\,\epsilon_2\cdot p_1}{M_\Theta^2-M_V^2}\right) \quad , \tag{C.1}$$

where μ_Θ is the scalar trilinear coupling, $\tilde{g}$ is the scalar-vector gauge coupling, M_V and M_Θ are the V_μ and scalar masses. The dimensionless coefficient $\mathcal{C}$ is the only quantity that needs to be computed from loop integrals.

We now compute the coefficient $\mathcal{C}$ for the process $\Theta^+\to W^+g$ by evaluating the 1-loop diagrams

$$\mathcal{M} = \int\frac{d^4k}{(2\pi)^4}\frac{48i\,\mu_\Theta g_s g}{(k^2-M_\varphi^2)[(p_1+p_2+k)^2-M_\varphi^2]} \times\left(\frac{1}{4}\,\epsilon_1\cdot\epsilon_2 - \frac{\epsilon_1\cdot(p_2+k)\,(\epsilon_2\cdot k)}{(p_2+k)^2-M_\varphi^2}\right) \quad , \tag{C.2}$$

where k is the loop 4-momentum and M_φ is the mass of the scalars running in the loop. The logarithmic divergences from the three diagrams cancel, and $\mathcal{C}$ in Eq. (C.1) can be written as a Feynman parameter integral

$$\mathcal{C} = \int_0^1 dx\int_0^{1-x} dy\,\frac{-3(1-R^2)\,xy}{1-xy-R^2\,x\,(1-x-y)} \quad . \tag{C.3}$$

with $R \equiv M_W/M_\varphi$. Here we have assumed $M_\varphi = M_\Theta$, as is the case for the octo-triplet (see Figure 1). After integration over y we obtain

$$\mathcal{C} = \frac{-3}{2(1-R^2)}\left[\frac{\pi^2}{9}-1+R^2\left(\frac{\pi}{\sqrt{3}}-1\right)+2J(R)\right], \tag{C.4}$$

where we have defined

$$J(R) = \int_0^1 dx\left(\frac{1}{x}-R^2\,x\right)\ln\left[1-R^2\,x(1-x)\right] \quad . \tag{C.5}$$

For $R \ll 1$ the function J has the form

$$J(R) = -\frac{R^2}{2}\left(1-\frac{R^2}{12}-\frac{R^4}{180}\right)+\mathcal{O}(R^8) \quad . \tag{C.6}$$

After squaring the amplitude (C.1) and summing over final state polarizations, we find the following decay width:

$$\Gamma(\Theta^+\to W^+g) = \frac{\alpha_s\alpha\,\mu_\Theta^2}{\pi^3\sin^2\theta_W M_\Theta}f(R) \quad , \tag{C.7}$$

where

$$f(R) = \frac{1}{2}\,\mathcal{C}^2(1-R^2) \quad , \tag{C.8}$$

with $\mathcal{C}$ depending on R as shown in Eq. (C.4). This function, which appears in all 1-loop decays discussed in this paper, is accidentally suppressed by cancellations between terms involving various powers of π. To see this, consider the expansion around $R \equiv M_W/M_\Theta \to 0$:

$$f(R) = f(0) + f_1 R^2 + f_2 R^4 + \mathcal{O}(R^6) \quad , \qquad \text{(C.9)}$$

Each of the above coefficients happens to be much smaller than order one:

$$\begin{aligned} f(0) &= \frac{9}{8}\left(\frac{\pi^2}{9} - 1\right)^2 \simeq 1.05 \times 10^{-2} \quad , \\ f_1 &= f(0) + \frac{9}{4}\left(\frac{\pi^2}{9} - 1\right)\left(\frac{\pi}{\sqrt{3}} - 2\right) \\ &\simeq -3.00 \times 10^{-2} \quad , \\ f_2 &= \frac{9}{8}\left(\frac{\pi^2}{9} + \frac{\pi}{\sqrt{3}} - 3\right)^2 + \frac{3}{16}\left(\frac{\pi^2}{9} - 1\right) \\ &\simeq 2.71 \times 10^{-2} \quad . \end{aligned} \qquad \text{(C.10)}$$

The above value of $f(0)$ agrees with that extracted from the width of an octo-doublet [13] or octo-singlet [2] decaying into gg.

Eqs. (C.7), (C.9) and (C.10) show that the 2-body decays of the octo-triplet into gauge bosons are suppressed by two orders of magnitude compared to estimates based on dimensional analysis.

References

[1] R. S. Chivukula, M. Golden and E. H. Simmons, "Multi - jet physics at hadron colliders," Nucl. Phys. B **363**, 83 (1991).

[2] B. A. Dobrescu, K. Kong and R. Mahbubani, "Massive color-octet bosons and pairs of resonances at hadron colliders," Phys. Lett. B **670**, 119 (2008) [arXiv:0709.2378 [hep-ph]].

[3] Y. Bai, B. A. Dobrescu, "Heavy octets and Tevatron signals with three or four b jets," [arXiv:1012.5814 [hep-ph]].

[4] CDF Collaboration, "Search for Higgs bosons produced in association with b quarks", Note 10105, June 2010, `http://www-cdf.fnal.gov/physics/new/hdg//Results_files/results/3b_susyhiggs_jun10`

[5] R. Boughezal, F. Petriello, "Color-octet scalar effects on Higgs boson production in gluon fusion," Phys. Rev. **D81**, 114033 (2010). [arXiv:1003.2046 [hep-ph]].
R. Boughezal, "Constraints on heavy colored scalars from Tevatron's Higgs exclusion limit," [arXiv:1101.3769 [hep-ph]].

[6] For a review, see C. T. Hill and E. H. Simmons, "Strong dynamics and electroweak symmetry breaking," Phys. Rept. **381**, 235 (2003) [Erratum-ibid. **390**, 553 (2004)] [arXiv:hep-ph/0203079].

[7] C. Kilic, T. Okui and R. Sundrum, "Colored Resonances at the Tevatron: Phenomenology and Discovery Potential in Multijets," JHEP **0807**, 038 (2008) [arXiv:0802.2568 [hep-ph]].
"Vectorlike Confinement at the LHC," JHEP **1002**, 018 (2010) [arXiv:0906.0577 [hep-ph]].

[8] Y. Bai and A. Martin, "Topological Pions," Phys. Lett. B **693**, 292 (2010) [arXiv:1003.3006].
Y. Bai and R. J. Hill, "Weakly interacting stable hidden sector pions," Phys. Rev. D **82**, 111701 (2010) [arXiv:1005.0008 [hep-ph]].

[9] G. Burdman, B. A. Dobrescu and E. Ponton, "Resonances from two universal extra dimensions," Phys. Rev. D **74**, 075008 (2006) [arXiv:hep-ph/0601186].

[10] M. V. Martynov and A. D. Smirnov, "Chiral color symmetry and possible G'-boson effects at the Tevatron and LHC," Mod. Phys. Lett. A **24**, 1897 (2009) [arXiv:0906.4525 [hep-ph]].

[11] A. V. Manohar and M. B. Wise, "Flavor changing neutral currents, an extended scalar sector, and the Higgs production rate at the LHC," Phys. Rev. D **74**, 035009 (2006) [arXiv:hep-ph/0606172].

[12] J. M. Arnold, M. Pospelov, M. Trott and M. B. Wise, "Scalar representations and minimal flavor violation," JHEP **1009**, 073 (2010). [arXiv:0911.2225 [hep-ph]].

[13] M. I. Gresham, M. B. Wise, "Color octet scalar production at the LHC," Phys. Rev. **D76**, 075003 (2007). [arXiv:0706.0909 [hep-ph]].

[14] M. Gerbush *et al.*, "Color-octet scalars at the LHC," Phys. Rev. **D77**, 095003 (2008). [arXiv:0710.3133].

[15] CDF Collaboration, `http://www-cdf.fnal.gov/physics/ewk/2011/wjj/7_3.html`, May 2011.

[16] T. Aaltonen *et al.* [CDF Collaboration], "Invariant Mass Distribution of Jet Pairs Produced in Association with a W boson in $p\bar{p}$ Collisions at $\sqrt{s} = 1.96$ TeV," arXiv:1104.0699.

[17] V. M. Abazov *et al.* [D0 Collaboration], "Study of the dijet invariant mass distribution in $p\bar{p} \to W(\to \ell\nu) + jj$ final states at $\sqrt{s} = 1.96$ TeV," arXiv:1106.1921 [hep-ex].

[18] F. Yu, "A Z' model for the CDF dijet anomaly," arXiv:1104.0243.
M. R. Buckley, D. Hooper, J. Kopp and E. Neil, "Light Z' bosons at the Tevatron," arXiv:1103.6035.
K. Cheung, J. Song, "Tevatron Wjj Anomaly and the baryonic Z' solution," arXiv:1104.1375.
X. P. Wang *et al,* "New color-octet vector boson revisit," arXiv:1104.1917; "O(100 GeV) deci-weak W'/Z' at Tevatron and LHC," arXiv:1104.1161.
L. A. Anchordoqui *et al,* "Stringy origin of Tevatron Wjj anomaly," arXiv:1104.2302.

[19] A. E. Nelson, T. Okui, T. S. Roy, "A unified, flavor symmetric explanation for the $t\bar{t}$ asymmetry and Wjj excess at CDF," arXiv:1104.2030.
C. Kilic and S. Thomas, "Signatures of resonant super-partner production with charged-current decays," arXiv:1104.1002.
E. J. Eichten, K. Lane and A. Martin, "Technicolor at the Tevatron," arXiv:1104.0976.

[20] R. Sato, S. Shirai, K. Yonekura, "A Possible Interpretation of CDF Dijet Mass Anomaly and its Realization in Supersymmetry," arXiv:1104.2014.

[21] S. Dodelson, B. R. Greene, L. M. Widrow, "Baryogenesis, dark matter and the width of the Z," Nucl. Phys. **B372**, 467-493 (1992).
M. Cirelli, N. Fornengo, A. Strumia, "Minimal dark matter," Nucl. Phys. **B753**, 178-194 (2006). [hep-ph/0512090].

[22] J. Alwall, M. Herquet, F. Maltoni, O. Mattelaer, T. Stelzer, "MadGraph 5 : Going Beyond," [arXiv:1106.0522 [hep-ph]].

[23] N. D. Christensen, C. Duhr, "FeynRules - Feynman rules made easy," Comput. Phys. Commun. **180**, 1614-1641 (2009). [arXiv:0806.4194]; FeynRules, version 1.6beta, `http://feynrules.irmp.ucl.ac.be/`;
Model files for heavy octets are available at `http://theory.fnal.gov/people/dobrescu/octet/`.

[24] J. Pumplin *et al.*, "New generation of parton distributions with uncertainties from global QCD analysis," JHEP **0207**, 012 (2002) [arXiv:hep-ph/0201195].

[25] Y. Kats, M. D. Schwartz, "Annihilation decays of bound states at the LHC," JHEP **1004**, 016 (2010). [arXiv:0912.0526 [hep-ph]].

[26] C. Kim, T. Mehen, "Color Octet Scalar Bound States at the LHC," Phys. Rev. **D79**, 035011 (2009). [arXiv:0812.0307 [hep-ph]].
A. Idilbi, C. Kim, T. Mehen, "Pair Production of Color-Octet Scalars at the LHC," Phys. Rev. **D82**, 075017 (2010). [arXiv:1007.0865].

[27] E. Gamiz *et al.* [HPQCD Collaboration], "Neutral B meson mixing in unquenched lattice QCD," Phys. Rev. D **80**, 014503 (2009) [arXiv:0902.1815 [hep-lat]].

[28] A. J. Buras, S. Jager and J. Urban, "Master formulae for $\Delta F = 2$ NLO-QCD factors in the standard model and beyond," Nucl. Phys. B **605**, 600 (2001) [arXiv:hep-ph/0102316].

[29] D. Becirevic *et al.*, "B-parameters of the complete set of matrix elements of $\Delta B = 2$ operators from the lattice," JHEP **0204**, 025 (2002) [arXiv:hep-lat/0110091].

[30] A. Lenz and U. Nierste, "Theoretical update of $B_s - \bar{B}_s$ mixing," JHEP **0706**, 072 (2007) [arXiv:hep-ph/0612167].

[31] B. A. Dobrescu, P. J. Fox, A. Martin, "CP violation in B_s mixing from heavy Higgs exchange," Phys. Rev. Lett. **105**, 041801 (2010). [arXiv:1005.4238 [hep-ph]].

[32] V. M. Abazov *et al.* [D0 Collaboration], "Evidence for an anomalous like-sign dimuon charge asymmetry," Phys. Rev. D **82**, 032001 (2010) [arXiv:1005.2757 [hep-ex]].

[33] CDF Collaboration, "Search for a new hadronic resonance using jet ensembles with CDF", note 10256, February 2011.

[34] T. Sjostrand, S. Mrenna and P. Skands, "PYTHIA 6.4 physics and manual," JHEP **0605**, 026 (2006). [arXiv:hep-ph/0603175].

[35] J. S. Conway, "Pretty Good Simulation of high-energy collisions", 090401 release, `http://physics.ucdavis.edu/~conway/` research/ software/pgs/pgs4-general.htm

[36] J. Thaler *et al*, Chameleon version 1.02, July 2006, `http://v1.jthaler.net/olympicswiki/doku.php?id=lhc_olympics:analysis_tools`.

[37] V. M. Abazov *et al.* [D0 Collaboration], "Measurement of the $t\bar{t}$ production cross section in $p\bar{p}$ collisions at $\sqrt{s} = 1.96$ TeV," Phys. Rev. Lett. **100**, 192004 (2008) [arXiv:0803.2779].
T. Aaltonen *et al.* [CDF Collaboration], "First measurement of the ratio $\sigma_{t\bar{t}}/\sigma_{Z/\gamma^* \to \ell\ell}$ and precise extraction of the $t\bar{t}$ cross section," Phys. Rev. Lett. **105**, 012001 (2010) [arXiv:1004.3224].

[38] S. Chatrchyan *et al.* [CMS Collaboration], "Measurement of the Top-antitop Production Cross Section in pp Collisions at $\sqrt{s} = 7$ TeV using the Kinematic Properties of Events with Leptons and Jets," [arXiv:1106.0902].
ATLAS Collaboration, "Measurement of the $t\bar{t}$ production cross-section in pp collisions at $\sqrt{s} = 7$ TeV using kinematic information of lepton+jets events", note ATLAS-CONF-2011-121, Aug. 2011.

[39] C. T. Hill, "Topcolor: Top quark condensation in a gauge extension of the standard model," Phys. Lett. **B266**, 419-424 (1991).

[40] L. J. Hall and A. E. Nelson, "Heavy gluons and monojets," Phys. Lett. B **153**, 430 (1985).

[41] CDF Collaboration, `http://www-cdf.fnal.gov/physics/ewk/2011/wjj/kinematics.html`, May 2011.